Urban Forestry & Urban Greening 20 (2016) 43–55

Contents lists available at ScienceDirect

Urban Forestry & Urban Greening

journal homepage: www.elsevier.com/locate/ufug

Regional variability in the impacts of future land use on summertime temperatures in Kanto region, the Japanese megacity

Yousuke Sato[a,*], Atsushi Higuchi[b], Akinori Takami[c], Akinobu Murakami[d], Yuji Masutomi[e], Kazuaki Tsuchiya[f], Daisuke Goto[c], Teruyuki Nakajima[g]

[a] RIKEN Advanced Institute for Computational Science, Kobe, Hyogo, Japan
[b] Center for Environmental Remote Sensing, Chiba University, Chiba, Japan
[c] National Institute for Environmental Studies, Tsukuba, Ibaraki, Japan
[d] Faculty of Engineering, Information and Systems, University of Tsukuba, Tsukuba, Ibaraki, Japan
[e] College of Agriculture, Ibaraki University, Inashiki-gun, Ibaraki, Japan
[f] Graduate School of Agricultural and Life Sciences, The University of Tokyo, Tokyo, Japan
[g] Earth Observing Research Center, Japan Aerospace Exploration Agency, Tsukuba, Ibaraki, Japan

ARTICLE INFO

Article history:
Received 29 January 2016
Received in revised form 19 July 2016
Accepted 28 July 2016
Available online 30 July 2016

Keywords:
Afforestation impacts
JMANHM
Regional variability of the impacts of afforestation
Urban area in Japan

ABSTRACT

Summer high temperatures affecting urban areas pose a significant problem to human health. The Japanese megacity, Tokyo Metropolitan Area (TMA) in Kanto region, where significant urban shrinkage is expected to occur in the coming decades, is also vulnerable to such temperature issues. We investigated the impacts arising from changes in land use on future maximum surface air temperature (T_{smax}) at the regional scale in Kanto region. For our numerical experiments, we introduced surface parameters (*i.e.*, albedo, evapotranspiration coefficient, and heat capacity) into the Japan Meteorological Agency Non-Hydrostatic Model (JMANHM), used for operational weather forecasts in Japan. The impacts were estimated regarding several urban planning scenarios, in which the micro scale afforestation in TMA was considered, *i.e.*, compact-city, dispersed-city, and active afforestation. The obtained results indicated that the afforestation might decrease T_{smax}, and active afforestation within a compact-city scenario was the most effective for reducing T_{smax} in Kanto region. Our findings also revealed a relatively smaller afforestation impact on T_{smax} values in the coastal areas (*e.g.,* Kanagawa) than those affecting inland regions (*e.g.,* Saitama and Tokyo). In coastal areas located upwind of Kanto region, only local afforestation affected T_{smax}. On the other hand, in inland zones, located on the downwind side of Kanto region, afforestation in both local and upwind areas contributed to a decrease in T_{smax}. Consequently, the impacts of afforestation were larger in inland areas.

1. Introduction

High summer temperatures are expected to occur in urban areas owing to the Urban Heat Island (UHI) effect and climate change (*e.g.,* global warming; Stocker et al., 2013). The high temperatures over urban areas cause significant human health problems, including heat stroke and higher prevalence of infectious diseases (*e.g.*, Ng et al., 2014), because about half of the population are living in an urban area (United Nations, 2015). To reduce the problems, political will is required to mitigate and adapt the high urban temperatures. From the 1990s, several methods have been proposed to mitigate high urban area temperatures, *e.g.*, increasing roof albedo (Krayenhoff and Voogt, 2010), changing pavement materials (Takebayashi and Moriyama, 2012), changing urban structures (Scherer et al., 1999), and greening (*e.g.,* afforestation) of building walls (*e.g.*, Onishi et al., 2010). One type of urban structure, the compact city, in which buildings are concentrated around the central area and residential density is high, is proposed for UHI based on an Ecological based Adaptation approach (EbA: Brink et al., 2016). The opposite structure to the compact city is urban sprawl (or suburban

* Corresponding author.
E-mail addresses: yousuke.sato@riken.jp (Y. Sato), higu@faculty.chiba-u.jp (A. Higuchi), takamia@nies.go.jp (A. Takami), murakami@sk.tsukuba.ac.jp (A. Murakami), yujim@mx.ibaraki.ac.jp (Y. Masutomi), aktcy@mail.ecc.u-tokyo.ac.jp (K. Tsuchiya), goto.daisuke@nies.go.jp (D. Goto), nakajima.teruyuki@jaxa.jp (T. Nakajima).

http://dx.doi.org/10.1016/j.ufug.2016.07.012

sprawl, dispersed city) in which urban area and human population spreads away from the central area.

The impacts of urban structure on surface air temperature (T_s) have been investigated by using meteorological models. Martilli (2014) investigated the effects of urban structure, assuming a large number of idealized urban structures, and indicated that the compact city has advantages for energy consumption, but it has disadvantage in terms of decreasing temperature. The effects have also been investigated in real urban cities, for example, Yang et al. (2016) investigated the effects of urban structure in Beijing, China.

For the Japanese megacity, Kanto region, which includes Tokyo Metropolitan Area (TMA), Adachi et al. (2014), Suzuki-Parker et al. (2015), and Kusaka et al. (2016) investigated the effects of urban structure by using a meteorological model coupled with an urban canopy model (UCM). Their studies used the urban planning scenarios of dispersed city and compact city based on Yamagata et al. (2011), which were created using a land use equilibrium model based on economic theory. They indicated that the compact city has advantages for reducing urban high temperature in nighttime over TMA. However Adachi et al. (2014) indicated that T_s was reduced in the compact city scenario when evaluated through the average temperature over whole TMA, but T_s at the central part of TMA was increased, even though the T_s in suburban areas was reduced. Kusaka et al. (2016) also indicated that the reduction of T_s near the center part of TMA by adopting the compact city was smaller than in the surrounding area. These results imply that the amplitude of the benefits, which are evaluated by the reduction in high temperature by adopting the compact city, was different from area to area in the Kanto region. Since adaptation policies are only achieved with the collaboration of all local autonomies in Kanto region, it is useful to estimate the regional variability in the benefits before discussing the costs attributable to each autonomy.

In view of urban planning, the effect of urban shrinkage on T_s needs to be accounted for, especially in developed countries (Emmanuel and Krüger, 2012). Considering the global abundance of shrinking cities, testing the relationships among urban shrinkages, greenings and T_s is a matter of growing relevance (Haase et al., 2014). Afforestation in the shrunken urban area, and increasing its green infrastructure (GI) (*e.g.*, vegetated roof, urban lawns, urban agriculture and so on), are other methods proposed to mitigate the UHI. That is because the suburban area available for afforestation and increasing GI will increase if urban buildings are concentrated through adopting the compact city (Conlon et al., 2016). Thus, understanding of the area in which additional afforestation or GI is possible, can provide useful information for government policy makers when they create policies for adaptation to high temperature. Such information is also useful to discuss the cost-effectiveness of afforestation, which is a crucial issue regarding urban planning development and implementation.

Within this background, the purpose of this study is to investigate the regional variability of the benefit of changing urban structure, and to investigate the distribution of the area, available for additional afforestation and GI, by numerical meteorological model experiment targeting Kanto region.

The Kanto region includes the largest urban area in the world, TMA, where urban shrinkage is expected. Thus, the findings from our numerical experiments will also be beneficial to other growing Asian megacities, where dominant contemporary urbanization is taking place (Seto et al., 2011), while sharing similar humid, hot summer weather conditions, and heat-related health to Tokyo (Tran et al., 2006). Here, we considered the impacts of daily maximum air temperature near the surface (T_{smax}) in summer, since the demand for medical care associated with heat stroke notably increases when apparent temperatures exceed 35 °C in Kanto region (Ng et al., 2014), close to the maximum summertime temperature.

Table 1
Summary of the model used in this study.

Component	Name and Reference
Governing equation system	Compressible
Time discretization	Horizontally explicit and vertically implicit (HE-VI)
Spatial discretization	4th order central differential scheme
Cloud microphysics	1-moment bulk microphysical scheme (Yamada, 2003)
Turbulence scheme	Mellor-Yamada type level 2.5 (Nakanishi and Niino, 2006)
Surface flux	Land (Louis, 1979), sea surface (Kondo, 1975)
Radiation	Kitagawa (2000)

2. Methodology

2.1. Model description and experimental setup

The meteorological model used in this study was the Non-Hydrostatic Model of Japan Meteorological Agency (JMANHM; Saito et al., 2006), which has been used for weather forecasting in Japan. The governing equation employed was the compressible non-hydrostatic equation, which predicts pressure, density weighted horizontal and vertical wind velocity, potential temperature, and the mixing ratio of vapor and hydrometeors. A horizontally explicit and vertically implicit (HE-VI) scheme, and 4th-ordered central differential scheme, was applied for temporal and spatial discretization respectively. To express the effects of turbulence, the spatial scale of which is usually smaller than grid spacing (i.e., 1 km in this study shown below), a turbulence scheme based on the Reynolds Averaged Navier-Stokes (RANS) model (Nakanishi and Niino, 2006) was used. We used a slab type surface model, in which the ground was divided into four layers, to predict ground temperature. The flux from surface to atmosphere (momentum flux, sensible heat flux, and latent heat flux) was calculated by a Louis type surface flux scheme (Louis, 1979). The bulk coefficient of each surface flux over land and sea was calculated using Louis (1979) and Kondo (1975) respectively. The roughness length over sea was changed based on the surface wind as in Kondo (1975). The physical processes of cloud microphysics and radiation were calculated by the 1-moment bulk microphysical scheme (Yamada, 2003), and a radiation scheme of Kitagawa (2000). The setting has been used for weather prediction near Japan (summary of the model is shown in Table 1).

We newly introduced the land use type for each grid to express the impact of urban planning, and such usage was classified according to seven categories (Table 2): forest, low tree and ground cover, low tree and multi-year ground cover, low tree and bare soil, urban, cultivation, and water (sea and river). The surface parameters of albedo (A), evapotranspiration (β), and heat capacity (C_h) for each land use type, determined following the methods of Kondo (1994) and Moriwaki et al. (2002), were introduced into the model. A surface roughness length of 0.1, and 0.002 for water, was used as the default value in JMANHM.

The initial and lateral boundary conditions of the model (horizontal wind; u and v, potential temperature; θ, vapor mixing ratio; q_v) were derived from Japan Meteorological Agency (JMA) MseoAnalaysis data (JMA-MANAL; 10 km resolution and 20 vertical layers up to 10 hPa). Vertical velocity (w) of the initial and lateral boundary was set to zero. Sea surface temperature (SST) was not included in JMA-MANAL, being instead taken from re-analysis data of the National Center for Environmental Prediction (NCEP; Kalnay et al., 1996). Since the time interval of JMA-MANAL and NCEP data was 6 h, lateral boundary data for u, v, θ, and q_v, and SST data were linearly interpolated.

Table 2
Land use type and surface parameters in JMANHM.[a]

Category	Land Use	Albedo (A)	Heat Capacity (C_h) [MJ K^{-1} m^{-3}]	Evapotranspiration Coefficient (β)
1	Forest	0.175	1.3	0.26
2	Low tree and ground cover	0.17	1.54	0.259
3	Low tree and multi-year ground cover	0.185	1.3	0.316
4	Low tree and bare soil	0.157	1.62	0.184
5	Urban	0.13	2.1	0.07
6	Cultivation	0.2	1.3	0.4
7	Water (Sea and River)	0.06	4.18	1.0

[a] Japan Meteorological Agency Non-Hydrostatic Model.

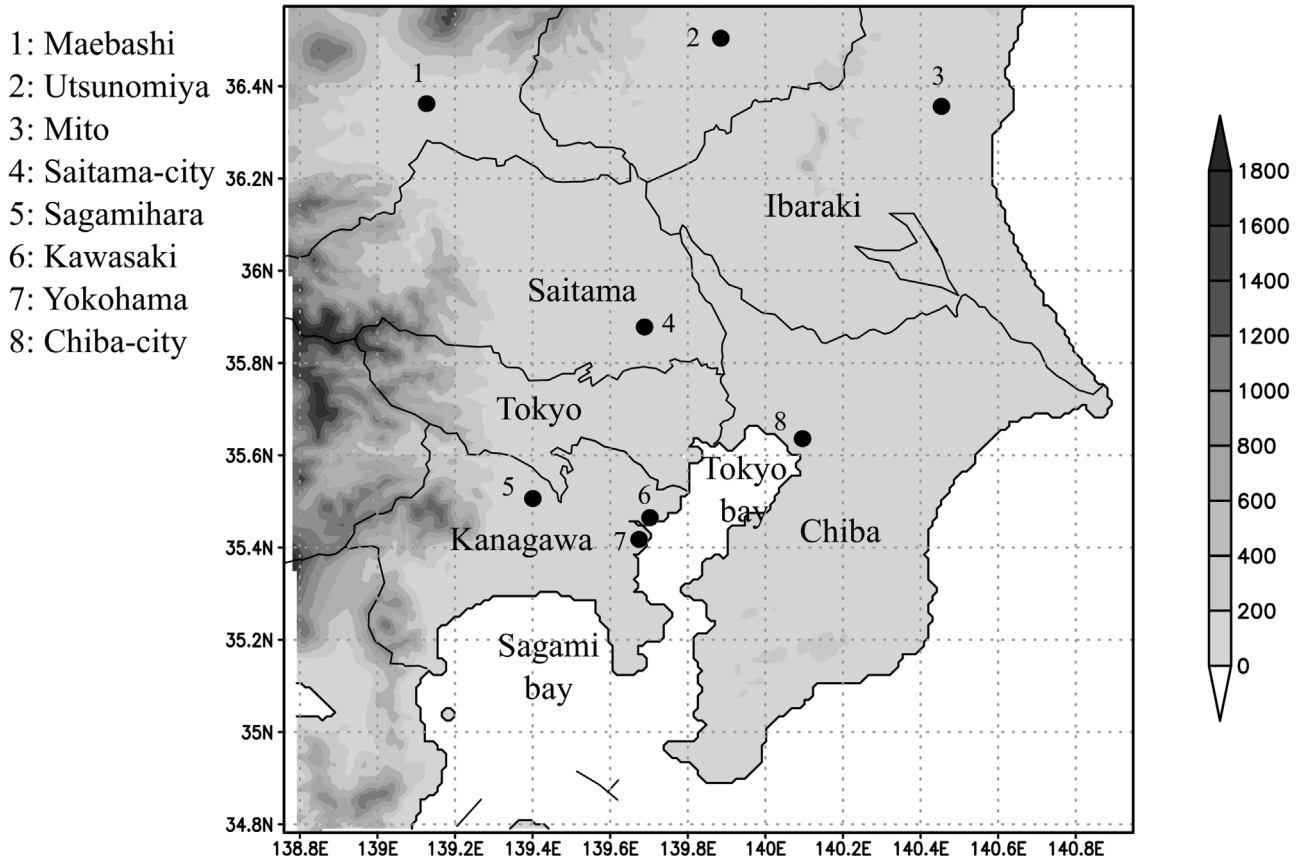

Fig. 1. Target domain of numerical simulation. Calculation domain denoting the elevation, name of each prefecture, bay, government-designated cities, and prefectural seats.

The calculation domain covered 200 × 200 km over the Kanto region (Fig. 1) with a horizontal grid spacing of 1 km (*i.e.*, 200 × 200 grids). The model contained 40 layers, with vertical grid spacing gradually increasing from 40 m at the surface to 1120 m at the model top (22400 m). We adopted Terrain-following (Gal-Chen and Somerville, 1975), and the GTOPO30 (U.S. Geological Survey, 1996) global digital elevation model was used for the elevation of each grid point. Time integration started at 00:00 Coordinated Universal Time (UTC) on August 7, 2007 and continued until 00:00 UTC on August 17, 2007, during which the highest recorded T_s (40.9 °C) occurred (Japan Meteorological Agency, 2008), with time steps (Δt) of 3 s.

2.2. Sensitivity experiments

Experiments assuming present conditions (CTL), four different future urban planning scenarios (VEG50, SPRAWL, COMPACT, and COMPACT30), and four sensitivity experiments (BAY-CTL, BAY-COMP30, BAY-CTL-SAGAMI, and ALBED) shown in Table 3, were conducted in order to validate the model and to investigate the variability of land use change impact on future T_s at the regional scale. With the exception of land use, the experimental setup was identical for all scenarios. The CTL corresponded to present day configurations (the control simulation), with a land use assumed from 2009 National Land Numerical Information (NLNI; National

Table 3
Scenario descriptions and names.

Description	Name
Land use in present day (control run)	CTL
Scenario: afforestation 50% of urban area	VEG50
Scenario: dispersed-city	SPRAWL
Scenario: compact-city	COMPACT
Scenario: compact-city scenario plus afforestation of 30% urban area	COMPACT30
Same as CTL but covering the Tokyo and Sagami bays with "Low tree and ground cover"	BAY-CTL
Same as COMPACT30 but covering the Tokyo and Sagami bays with "Low tree and ground cover"	BAY-COMP30
Same as BAY-CTL but locating a large urban area over Sagami Bay	BAY-CTL-SAGAMI
Same as CLT but with urban albedo changed to 0.246	ALBED

Land Information Division National Spatial Planning and Regional Policy Bureau MILT of Japan, 1997). The VEG50 scenario corresponded to an urban plan in which 50% of the current (*i.e.,* the CTL) urban area underwent afforestation. Even though such afforestation extent is unrealistic, this experiment was conducted to check the model response to extreme land use change and to investigate the geographical distribution of the area where additional GI and afforestation is possible.

The SPRAWL and COMPACT scenarios conformed to the two types of future urban design of Kanto region (Yamagata et al., 2011) in which significant shrinkage of urban area and reduction of population are expected to occur in the coming decades (Ariga and Matsuhashi, 2012): dispersed-city and compact-city, respectively. The former included the extension of residential and business areas from the urban center to the suburbs, while in the latter, residential, and business areas were concentrated near stations. The COMPACT30 scenario involved the COMPACT scenario with an additional 30% afforestation.

Since 30% afforestation is not always feasible in view of the involved economic costs, an alternative mitigation approach involves enhancing the albedo of urban areas by coating roofs with highly reflective material (Krayenhoff and Voogt, 2010). To test this method, we conducted a sensitivity experiment (ALBED) in which urban albedo was changed from the default value (A_{urban} = 0.13) to A'_{urban} (=0.246). The value of A'_{urban} was expressed as

$$A'_{urban} = A_{urban} \times (1 - S_{able}) + A_{high} \times S_{able}, \quad (1)$$

where S_{able} (=0.4) is the proportion of urban area suitable for coating with highly reflective material, and A_{high} (=0.42) the albedo of the highly reflection material.

Additionally, we conducted three sensitivity experiments to investigate the effects of maritime air masses transported from Tokyo and Sagami bays into Kanagawa. For the BAY-CTL and BAY-COMP30 scenarios, land uses were the same as CTL and COMPACT30, respectively, except for the conversion of the two bays from water into low tree and ground cover. Finally, the BAY-CTL-SAGAMI scenario was the same as BAY-CTL, with the Sagami Bay area converted to a large urban area.

2.3. Determination of land use

The categorization of land use in each grid was determined using the method described as follows (Fig. 2). The threshold values in Fig. 2 were determined from a large amount of sensitivity analyses. Firstly, grids containing more than 80% forested area were categorized as "forest." Grids with 40–80% forested area and proportion of green areas (*i.e.*, paddy, agricultural land, waste land, and golf course) higher and lower than 50% were classified as "low tree and multi-year ground cover" and "low tree and bare soil," respectively. Grids containing less than 20% forested area, and more than 50% cultivated land (*i.e.,* paddy and agricultural land) were labeled as "cultivation." Grids containing less than 20% forested area and less than 50% cultivated land were divided into two categories, based on the area of artificial buildings and sandy beach. The grids with more or less than 50% artificial buildings/sandy beach were categorized as "urban" and "water," respectively.

Grids with 20–40% forest area were divided into four categories. Grids where the proportion of green area was higher than 50%, and cultivated area was either higher or lower than 60% were categorized as "cultivation" and "low tree and ground cover," respectively. Grids where the proportion of green area was lower than 50% and the area of artificial building and sandy beach either higher or lower than 50% were classified as "urban" or "water," respectively. The basic geographical distribution of urban areas at the present day was well reproduced (Fig. 3a) by employing these categorizations.

For the VEG 50 scenario, 50% of the NLNI artificial building area in the government-designated cities (Kawasaki, Sagamihara), prefectural seats (Utsunomiya, Saitama, Chiba, Maebashi, Mito, and Yokohama), and 23 wards of Tokyo (covering almost all east part of Tokyo) of the CTL were converted into "forested area" (Fig. 3b).

To determine land use in the SPRAWL, COMPACT, and COMPACT30 scenarios, we calculated the population in 2050 (P_{2050}) in each grid, employing the method of Ariga and Matsuhashi (2012). The "Decentralized" and "Centralized" city scenarios of Ariga and Matsuhashi (2012) were assumed to correspond to our SPRAWL and COMPACT scenarios, respectively. Based on the populations in 2010 (P_{2010}) and P_{2050}, the ratios of forest (F_{2050}) and buildings (B_{2050}) were calculated for each grid:

$$B_{2050} = B_{2009} \times (1 + [P_{2050} - \mathrm{P}_{2010}]/\mathrm{P}_{2010}) \quad (2)$$

$$F_{2050} = F_{2009} - (\mathrm{B}_{2050} - \mathrm{B}_{2009}). \quad (3)$$

It is worth noting that F_{2050} in the grid where the population was expected to increase in 2050 was set to the same value as F_{2009}. The land use for COMPACT30 scenario was determined by converting 30% of the NLNI artificial building area into "forested area" in the government-designated cities, the prefectural seats, and 23 wards of Tokyo in COMPACT (Fig. 3e).

When considering the impacts arising from future changes in land use, we used averaged temperatures at a 2 m height (T2m) over sub domains defined as $5 \times 5\,\mathrm{km}^2$ grids (*i.e.,* 25 grids). The afforestation (or greening) ratio (G) of each sub domain, useful for estimating impacts, was defined as

$$G = V_s/\mathrm{N_g}, \quad (4)$$

where N_g is the number of grids in each sub domain (*i.e.*, 25 grids), and V_s the number of grids whose land use was converted from urban to vegetated area in each scenario.

2.4. Observational data

To confirm the validity of the model, we compared T2m results calculated by the model with temperatures obtained from the JMA Automated Meteorological Data Acquisition System (AMeDAS). To exclude discrepancy effects between AMeDAS points and the model grids, T2m was averaged using the nearest grid to the AMeDAS point and eight radial grids (*i.e.*, 9-grid averaged temperature), for comparison purposes. T2m was calculated from the temperatures of the modeled lowest layer, using the method of Adachi et al. (2014). In this study, modeled T_s and T_{smax} were considered equivalent to T2m and daily maximum value of T2m, respectively.

3. Results

3.1. Model evaluation

Firstly, we confirmed if the model was able to reproduce the T_{smax} observed from the AMeDAS (Fig. 4a and b). The results showed that the model underestimated T_{smax} over the northwestern part of Saitama and Gunma. Based on the analysis of Sakurai et al. (2009), the high temperatures of August 2007 were mainly caused by a Foehn generated by a northerly wind. However, the model did not reproduce the Foehn because the calculation domain did not cover the mountainous area of northern Kanto, giving rise to the temperature underestimation. Except for Gunma and northwestern Saitama, the contrasts in T_{smax} between coastal (Chiba, Kanagawa, and Ibaraki) and inland areas (Tokyo and Saitama) were well reproduced. The performance of the model was also tested using the relationship between the modeled daily T_{smax} and AMeDAS observational data (Fig. 4c). From these results, we concluded that the model was able to reproduce the T_{smax} trend of the Kanto region.

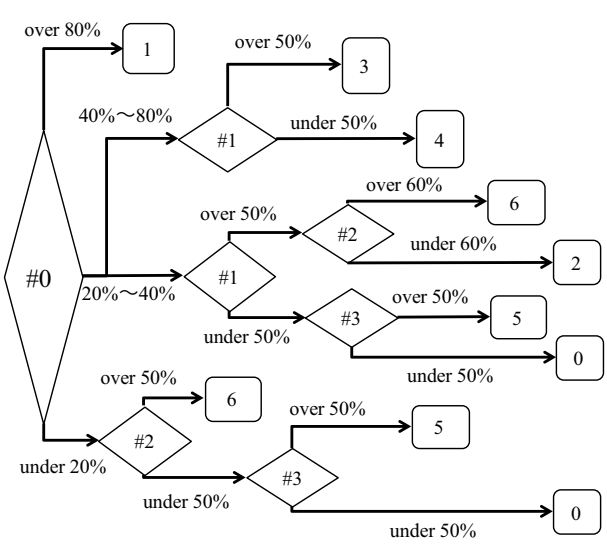

	Category
0	Water
1	Forest
2	Low tree and ground cover
3	Low tree and multi layer tree
4	Low tree and Bare Soil
5	Urban
6	Cultivation

#0 Ratio of forest area
#1 Ratio of green area for whole land except for forest (cultivated land + paddy + golf field)
#2 Ratio of cultivated land for whole land except for forest (cultivated land + paddy)
#3 Artificial building and sandy beach

Fig. 2. Summary of the method for land use categorization. Schematic illustration of the method used for land use categorization.

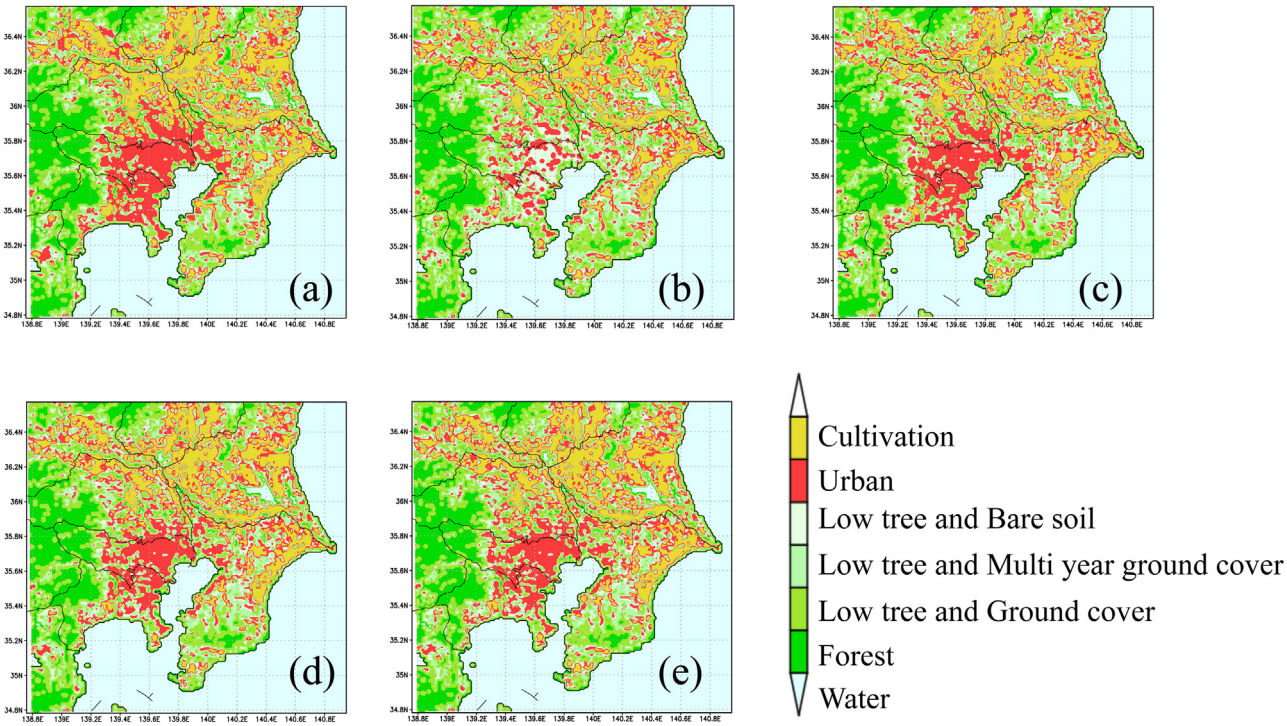

Fig. 3. Land use for each scenario experiment. Land use geographical distribution generated with scenarios (a) CTL, (b) VEG50, (c) SPRAWL, (d) COMPACT, and (e) COMACT30. For scenario descriptions, see Table 3. (This figure is monochrome in printed version. For interpretation of the references to colour in this figure legend, the reader is referred to the web version of this article.)

3.2. Geographical distribution of the area where adding GI and afforestation is possible

To test the capability of the model to express the impacts of land use change on T_s, we compared the CTL results with those of VEG50. Since this study targets high temperatures over the residential area, only land T_{smax} is discussed below. Fig. 5 shows the geographical distribution of differences in T_{smax} (henceforth referred to as ΔT_{smax}) between the CTL and VEG50 over the last 9 simulated days. As we discuss in Appendix A, the variation in T_{smax} was due to the conversion of surface heat flux from sensible heat flux to latent heat flux, which was similar to that found in the literature. The geographical distribution of the ΔT_{smax} was used as an indicator of the potential for increasing afforestation without considering the feasibility.

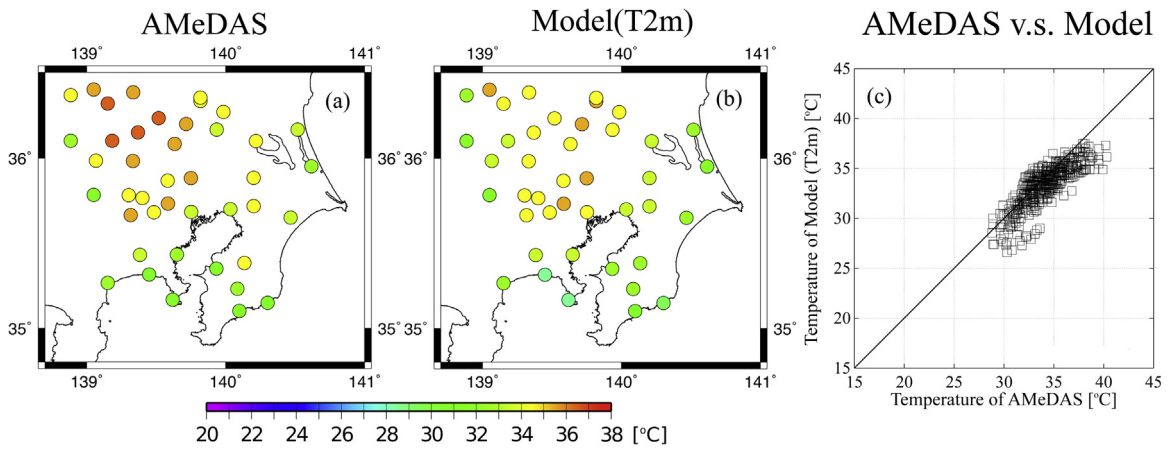

Fig. 4. Comparison between the results from the model and the observation. Geographical distribution of (a) daily maximum surface temperature observed by the Japan Meteorological Agency Automated Meteorological Data Acquisition System (AMeDAS), (b) model-derived daily maximum temperature at 2 m height (T2m) averaged over 10 days, and (c) scatter plot of daily maximum temperature from AMeDAS and Japan Meteorological Agency Non-Hydrostatic Model (JMANHM). (This figure is monochrome in printed version. For interpretation of the references to colour in this figure legend, the reader is referred to the web version of this article.)

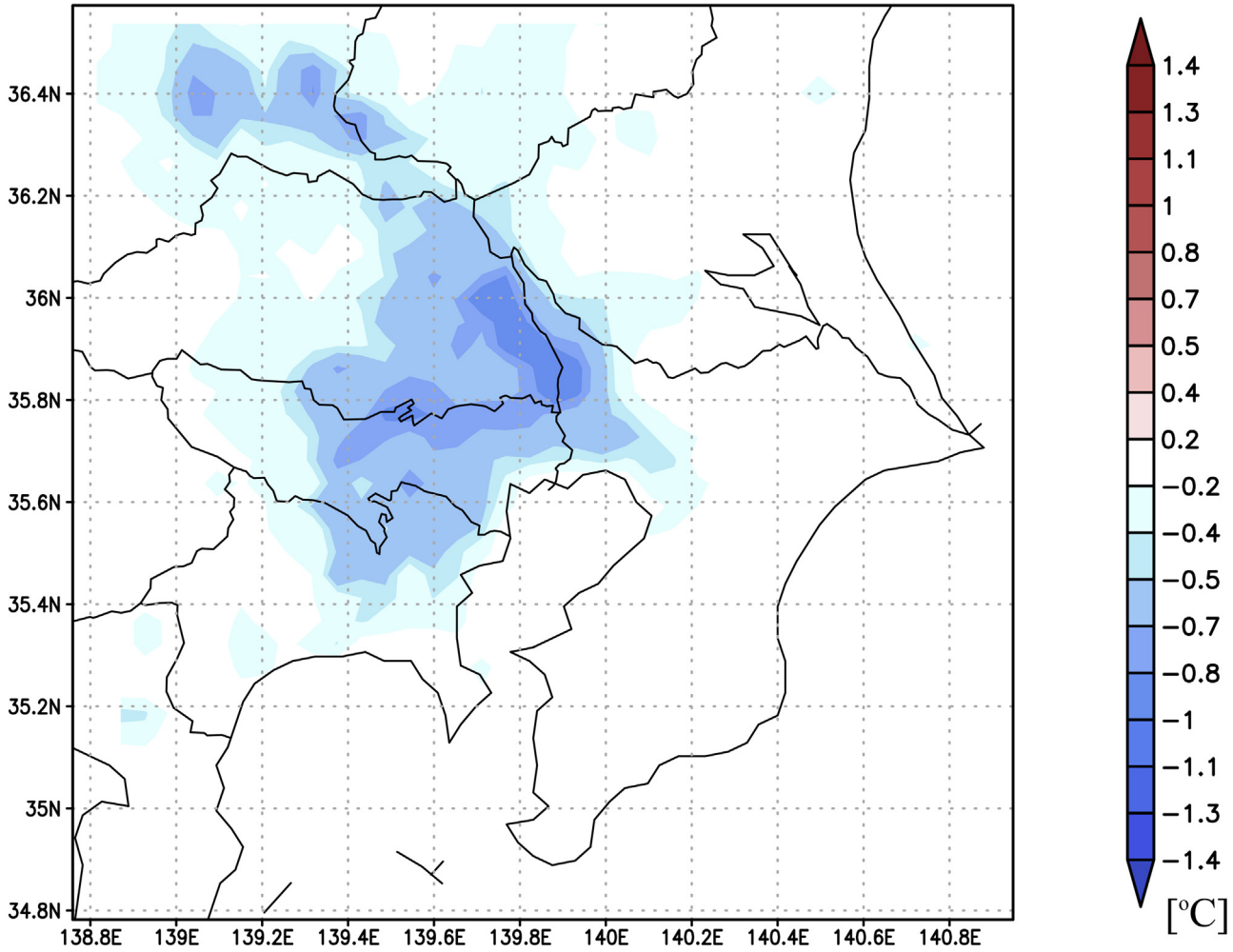

Fig. 5. Geographical distribution of the difference of T_{smax} by afforestation. Difference in daily maximum surface air temperature in each sub domain (5×5 km^2 width) over the land between the CTL and VEG50 scenarios ($T_{smax,VEG50} - T_{smax,CTL}$) averaged over the final 9 days of the simulation. For scenario descriptions, see Table 3. (This figure is monochrome in printed version. For interpretation of the references to colour in this figure legend, the reader is referred to the web version of this article.)

T_{smax} clearly decreased in the western part of Kanto region (*i.e.*, Tokyo, Kanagawa, and Saitama), and the maximum ΔT_{smax} was approximately −1.5 °C (Fig. 5). On the other hand, a small change in T_{smax} was observed in the eastern part of Kanto region (*i.e.*, Chiba, and Ibaraki). In the eastern part of Kanto region, urban area is small in the CTL and there is little room for afforestation. Over the western part of Kanto region, in contrast, there is wide area over which increasing GI or additional afforestation is possible. This area has

Table 4
Mean daily maximum temperature, vegetated area, and fitting line slope between ΔT_{smax} and G.[a]

Scenario	Daily Maximum Temperature at 2 m (9-day mean) [°C]	Vegetated Area [km^2]	Slope of Fitting Line Between ΔT_{smax} and G [°C km^{-2}]
CTL	30.450	–	–
SPRAWL	30.407	1165	−0.8234
COMPACT	30.403	1444	−0.8859
COMPACT30	30.377	1785	−0.8866
ALBED	30.344	4884[b]	−0.2640

[a] ΔT_{smax} = daily maximum surface temperature; G = afforestation (greening) ratio.
[b] Urban area across which albedo was changed.

been urbanized since the 1950s (Kusaka et al., 2000); such areas should be mainly targeted for mitigating the UHI in Kanto region.

In practice, it is difficult to uniformly increase the GI over whole urban area, and therefore, further investigation of feasible scenarios is required. This is discussed in the next section.

3.3. Scenario experiment results

In this section, we discuss the impact of afforestation based on the feasible scenarios (*i.e.*, SPRAWL, COMPACT, COMACT30). For the SPRAWL and COMPACT scenarios, T_{smax} decreased in eastern Saitama, and the area of negative ΔT_{smax} was more broadly distributed in COMPACT than in SPRAWL (Fig. 6). As we discussed in the previous section, T_{smax} was reduced around the urban area in CTL, in the western part of Kanto region. The negative ΔT_{smax} area was further extended into the Tokyo area in the COMPACT30 scenario. Overall, in terms of ΔT_{smax} magnitude averaged for the whole domain, SPRAWL yielded the smallest variation, followed by COMPACT, and COMPACT30. These results point toward the higher effectiveness of a compact-city configuration in mitigating high urban temperatures than a dispersed one, regarding the case of Kanto region. This is consistent with the results of Adachi et al. (2014), who showed that a compact-city can effectively reduce high nighttime temperatures. The area with ΔT_{smax} was smaller in Tokyo for the SPRAWL and COMPACT scenarios because the urban area remained unchanged. Reducing the urban area of central Tokyo is not a feasible planning option to decrease future T_{smax}. Therefore, afforestation or increasing GI is required to accomplish such a temperature reduction (*e.g.,* COMPACT30).

The number of grids where land use was converted from urban in CTL to vegetation in each scenario (henceforth referred to as vegetated grids) represented a good indicator of variability in ΔT_{smax} among the experiments (Table 4), with greater numbers of vegetated grids associated to larger decreases in ΔT_{smax}. For compact-city scenarios, the urban area was concentrated and the number of vegetated grid was larger than in dispersed-city scenarios. Thus, the COMPACT30 was most effective in decreasing T_{smax}, followed by COMPACT, and SPRAWL.

Actually, the difference between the T_s of compact city and that of dispersed city is determined by many factors (*i.e.*, urban morphology, surface vegetation fraction, heterogeneity of the urban area, and so on) (Aoyagi and Seino, 2011; Adachi et al., 2014; Theeuwes et al., 2014; Song and Wang, 2015; Kusaka et al., 2016). In this study, we only investigated the effects of change in the vegetation fraction, which was expressed in each 1×1 km grid, and ΔT_{smax} was mainly determined by the number of vegetated grids (Table 4). The absolute value of ΔT_{smax} may be changed when we implement the other factors.

A meteorological model coupled with an UCM is a powerful tool to examine ΔT_{smax} in more detail. We aim to conduct such a simulation by using JMANHM coupled with UCM (Aoyagi and Seino, 2011) in the near future. However, in this study we were able to find some insights from investigation of the geographical distribution of ΔT_{smax} and afforested grid as discuss below.

The relationship between ΔT_{smax} and G in each subdomain (Fig. 7) showed that a large G was related to a significant decrease in T_{smax} over the subdomain, while the slope between ΔT_{smax} and G was similar for all three scenarios. These results revealed that the number of vegetated grids controlled the magnitude of ΔT_{smax}. Hence, the SPRAWL scenario was deemed ineffective due to its small number of vegetated grids.

Despite the effectiveness of COMPACT30, achieving its land use in the real world would be challenging, especially owing to the economic costs associated with afforestation in an urban area. As discussed, an alternative method to mitigate UHI involves painting urban roofs with highly reflective material (Krayenhoff and Voogt, 2010). In the ALBED scenario, urban areas had higher albedo than those in CTL, and the heat absorbed by the surface was lower (Fig. 8). The domain mean ΔT_{smax} was ~0.1 °C (Table 4), similar to that of COMPACT30. Therefore, painting roofs with high albedo materials represents a potentially effective method for mitigating high temperatures in the Kanto region.

3.4. Regional variability in the impact of land use change

The impacts of land use change varied even at constant G (Fig. 7). Fig. 9 depicts the geographical distribution of ΔT_{smax} anomalies from the mean value of each experiment, corresponding to the regression line in Fig. 7. When the area north of 36.5°N was disregarded (*i.e.,* where the effects of lateral boundary conditions were significant), the impacts were greater (corresponding to a positive ΔT_{smax} anomaly) in inland areas and smaller (negative ΔT_{smax} anomaly) in coastal regions (*e.g.,* Kanagawa) regardless of the scenario.

In coastal areas, a maritime air mass was transported by a southwesterly wind from Tokyo and Sagami bays throughout the simulation time, significantly affecting temperatures. However, the effects of the maritime air mass were smaller in inland areas, with the resulting regional variability of ΔT_{smax}. To investigate the effects of this air mass, we conducted additional sensitivity experiments using the BAY-CTL and BAY-COMP30 scenarios, the land uses of which are shown in Fig. 10a and b, respectively. In these experiments, the effects of maritime air were small in Kanagawa, since the two bays did not exist and were thus not considered. The geographical distributions of the ΔT_{smax} and ΔT_{smax} anomaly between BAY-CTL and BAY-COMP30 were almost the same as between CTL and COMPACT30 (Fig. 11a and b). The spatial distribution of prevailing winds in BAY-CTL and BAY-COMP30 were also the same as in CTL and COMPACT30, respectively. The effects of afforestation were small in coastal and large in inland areas, despite the removal of the maritime air mass. Therefore, we conclude that the maritime air mass exerts a limited influence on T_{smax}.

The geographical orientation with respect to the prevailing wind (*i.e.*, southwesterly wind) was also different in each domain. Among afforested areas, the coastal portion was located upwind while the inland areas were mainly located in the downwind region. To unravel the influence of geographical location, a sensitivity experiment of the BAY-CTL-SAGAMI, the land use of which is shown as Fig. 10c, was conducted. Since the coastal area of Kanagawa was not the afforested region farthest upwind in BAY-CTL-SAGAMI, the location effect was reduced in this scenario. The 9-day ΔT_{smax} averages between BAY-CTL-SAGAMI and BAY-COMP30, and the mean ΔT_{smax} anomaly indicated that the number of areas with negative anomaly decreased in the coastal vicinities of Kanagawa (Fig. 11c and d). Furthermore, the ΔT_{smax} of urbanized areas over Sagami Bay gradually increased from upwind to downwind regions (Fig. 11c and d). These results show that the longer an air mass travels through the afforested area, the larger the resulting negative

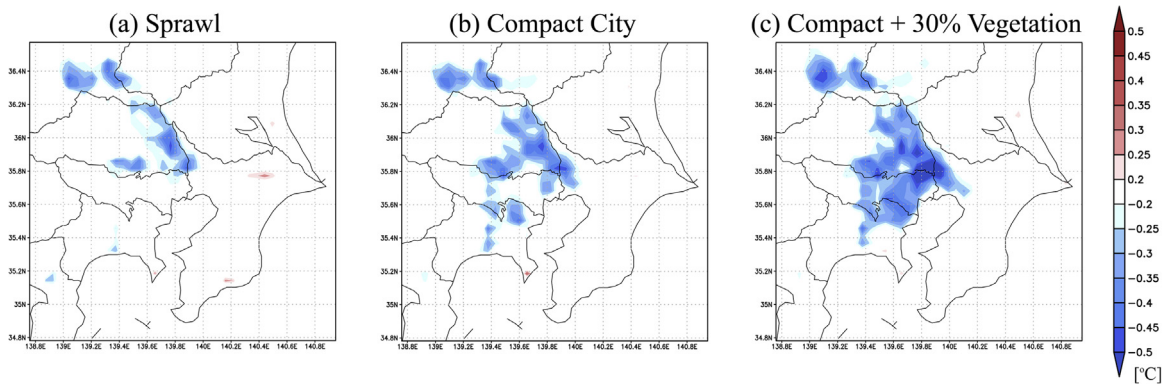

Fig. 6. Geographical distribution of the difference of T_{smax} by changing urban form and afforestation. Difference in daily maximum surface air temperature in each sub domain ($5 \times 5\,km^2$ width) over the land between the CTL and (a) SPRAWL, (b) COMPACT, and (c) COMPACT30 scenarios ($T_{smax,***} - T_{smax,CTL}$), averaged over the final 9 days of the simulation. For scenario descriptions, see Table 3. (This figure is monochrome in printed version. For interpretation of the references to colour in this figure legend, the reader is referred to the web version of this article.)

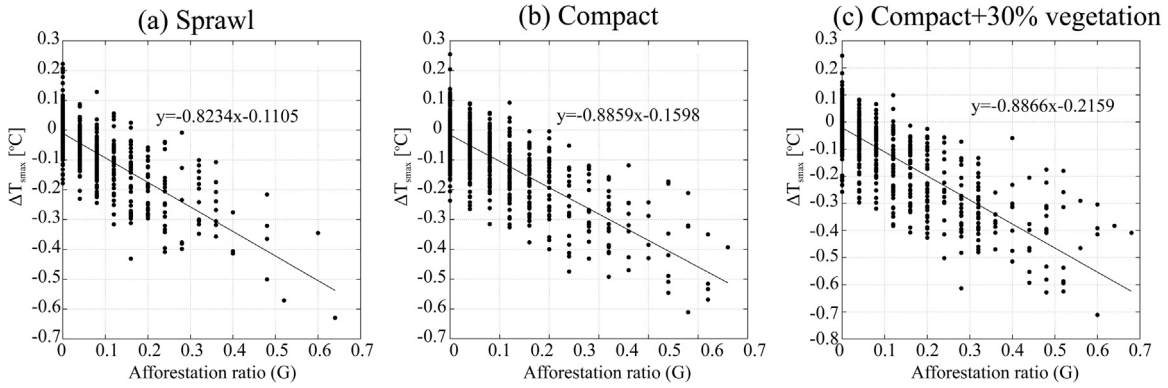

Fig. 7. Relationship between the afforestation ratio and difference in T_{smax}. Scatter plots between the afforestation (greening) ratio (G) and the differences in surface temperature between the CTL scenario and the (a) SPRAWL, (b) COMPACT, and (c) COMPACT30 scenarios.

ΔT_{smax}. Small negative ΔT_{smax} in coastal Kanagawa arose from its geographical orientation with respect to the general wind pattern. The large negative ΔT_{smax} of inland Saitama and Tokyo reflected the impacts of both local and coastal Kanagawa afforestation. These results show that afforestation in coastal Kanagawa would decrease high temperatures in inland areas during typical summer seasons (*e.g.*, when southwesterly winds are dominant).

4. Discussion

4.1. Mechanisms of regional variability

Our results showed that ΔT_{smax} in the Saitama and Tokyo areas partially resulted from land use change in upwind regions (*e.g.*, Kanagawa), indicating that the distance travelled by an air mass is a key factor in determining the magnitude of impact on surface temperature. Monteith (1965) has described a similar mechanism, taking into consideration the relationship between evaporation fluxes from the surface and total mean vapor concentration in the atmosphere. He used a 1-dimensional model with constant prevailing wind, in which vapor flux from the surface rose up to a point and then gradually decayed with distance, from upwind to downwind. In the upwind area, water vapor flux and concentration were large and small, respectively. On the other hand, the downwind region had larger vapor concentrations, despite a small vapor flux, since upwind emissions were accumulated downwind. The mechanism behind the regional variability in ΔT_{smax} observed for Kanto region was similar to that controlling the vapor emissions and total vapor mass concentrations registered by Monteith (1965). This mechanism was also suggested by Kusaka et al. (2000), who showed that the warming effects of UHI were more significant above downwind areas (*e.g.*, Saitama) than above upwind areas of Tokyo. They suggested that cumulative heat north of Tokyo was larger than that in Tokyo. The same mechanism was reflected in the impacts of land use change in the present study.

4.2. Necessity of sophisticated models to express urban canopy

Best and Grimmond (2015) emphasized the necessity of using the urban canopy model to reproduce urban area temperatures in Australia, and several simulations have been conducted for the Kanto region using a meteorological model coupled with UCM (*e.g.*, Aoyagi and Seino, 2011; Adachi et al., 2012, 2014; Aoyagi et al., 2012; Kusaka et al., 2012). Using the UCM, we can examine the impacts of several characteristics of the urban canopy, including urban morphology (Wang et al., 2013; Song and Wang, 2015), building aspect ratio (Aoyagi et al., 2012), radiative impacts such as shading effect (Theeuwes et al., 2014), effects of green roof, pavement, urban irrigation, and urban oasis (Yang and Wang, 2014; Yang et al., 2015), and artificial heat (Shrestha et al., 2008). All of these have been implemented in Weather Research and Forecasting (WRF, Skamarock et al. 2008). Investigations of urban effects, including some targeting the TMA, were initiated by Kusaka et al. (2016). They also compared the results of WRF and JMANHM coupled with an UCM, and both models showed similar results. We aim to conduct the same simulation using JMANHM coupled with UCM in future.

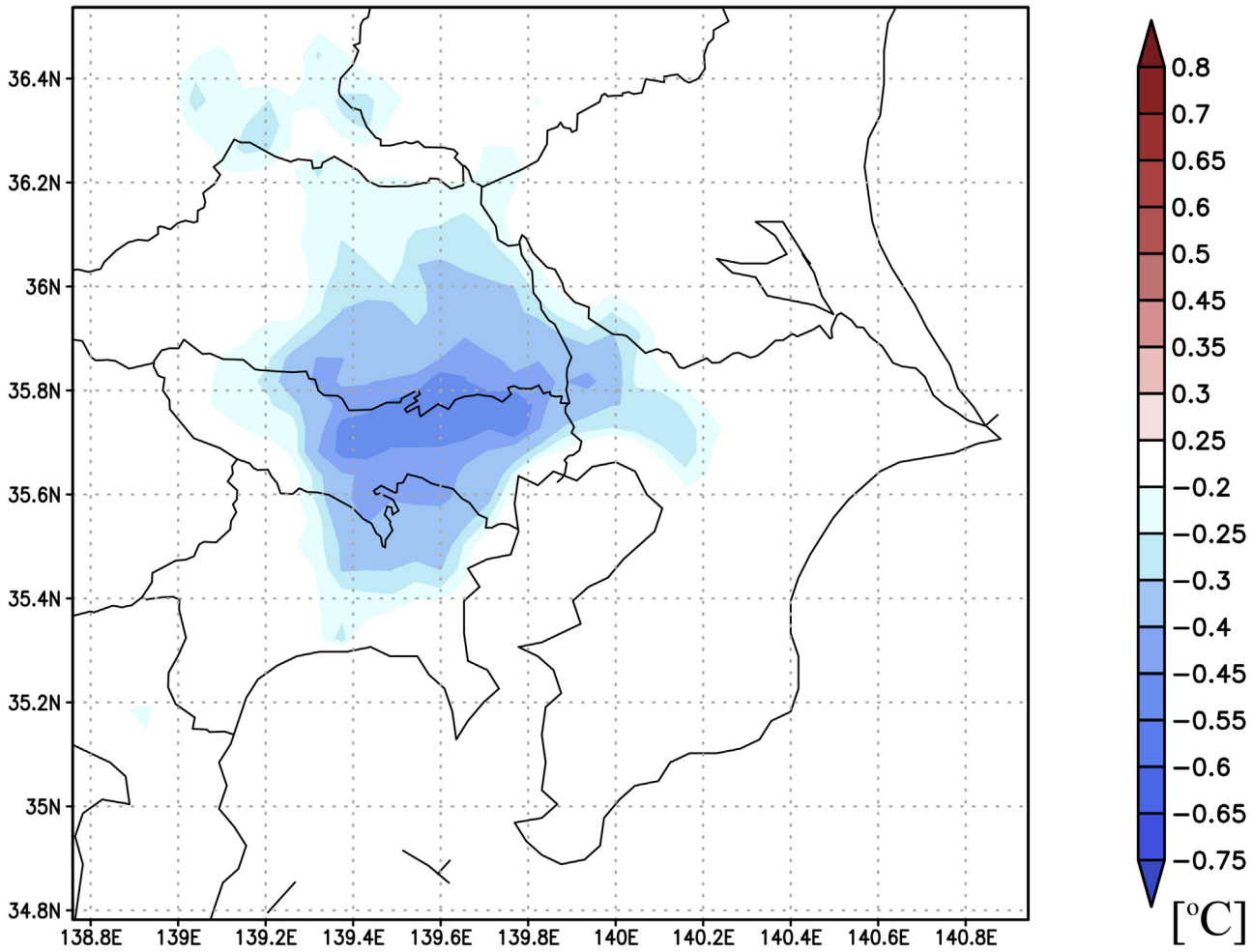

Fig. 8. Geographical distribution of the difference of T_{smax}. Difference in daily maximum surface temperature in each sub domain ($5 \times 5\,km^2$ width) over the land between the CTL and ALBED scenarios ($T_{smax,ALBED} - T_{smax,CTL}$) averaged over the final 9 days of the simulation. For scenario descriptions, see Table 3. (This figure is monochrome in printed version. For interpretation of the references to colour in this figure legend, the reader is referred to the web version of this article.)

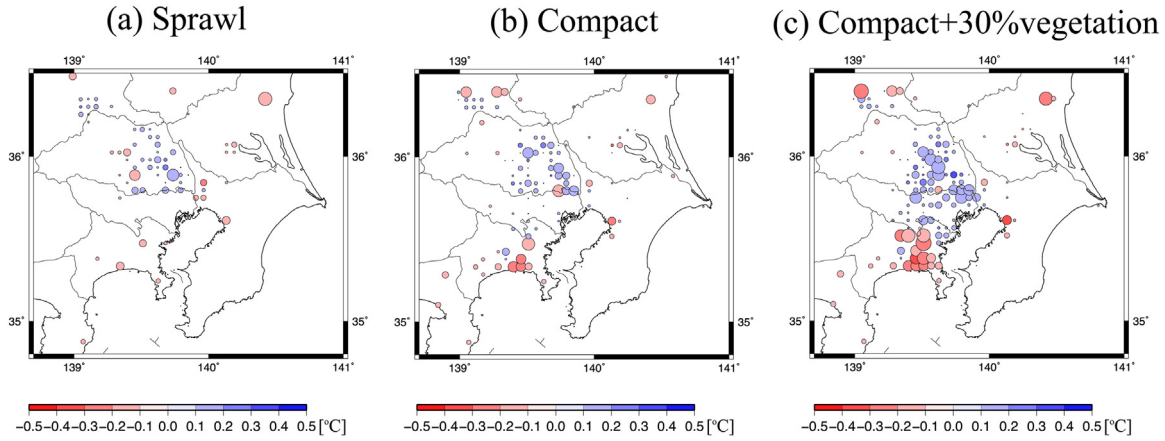

Fig. 9. Geographical distribution of the anomaly of mean daily maximum surface temperature (ΔT_{smax}) for each scenario experiment. Geographical distribution of afforestation (greening) ratio (G; shown by circle size) and the anomaly of mean daily maximum surface temperature (ΔT_{smax}), where red and blue denote ΔT_{smax} smaller and larger than the mean value, respectively, for (a) SPRAWL, (b) COMPACT, and (c) COMPACT30 scenarios. For scenario descriptions, see Table 3. (This figure is monochrome in printed version. For interpretation of the references to colour in this figure legend, the reader is referred to the web version of this article.)

Although this study ignored the effects of the detailed elements of the urban landscape, knowledge of the regional variability of ΔT_{smax} as discussed in Section 3.4 is meaningful for determining cost-effective afforestation or urban planning. In addition, the UCM may create further uncertainties in simulation results. UCM-combined simulations require larger computational resources, compared with the modeling methodology employed in this study. The simple method used to express the urban environment used here is sufficient to conduct the large number of experiments required in urban planning development.

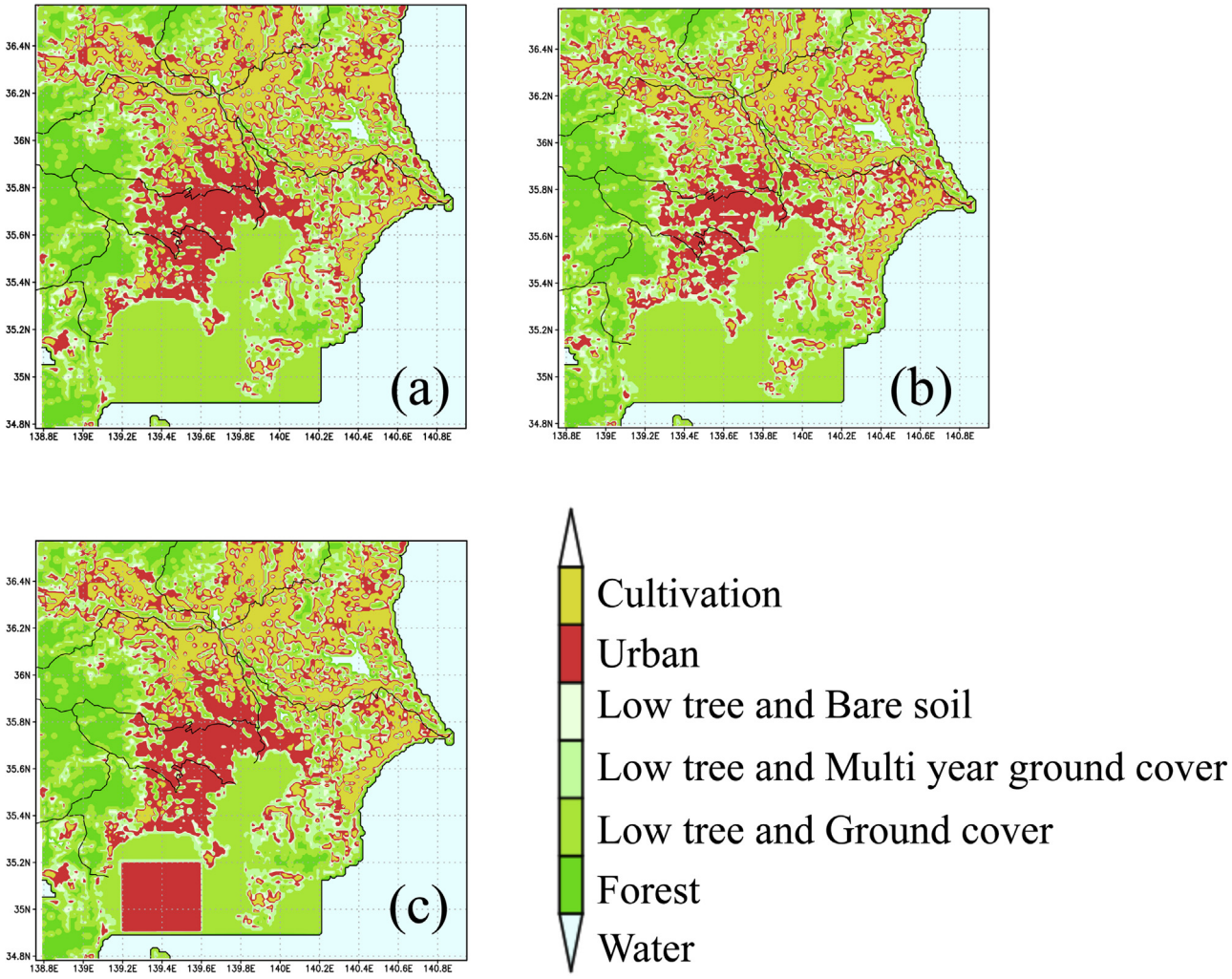

Fig. 10. Land use for each sensitivity experiment. Same as Fig. 3 but for (a) BAY-CTL, (b) BAY-COMP30, and (c) BAY-CTL-SAGAMI. (This figure is monochrome in printed version. For interpretation of the references to colour in this figure legend, the reader is referred to the web version of this article.)

4.3. Urban planning considerations

Our simulations indicated that a compact-city configuration would be more effective than a dispersed-city configuration for reducing high temperatures in Kanto region. However, the incurred economic costs, and practical feasibility, of achieving each scenario were not appraised. Our simulations showed that changing the roof albedo of urban buildings would also effectively reduce urban temperatures. However, we changed the albedo of all urban grids based on the assumption that buildings in $1 \times 1\,km^2$ areas were uniform, which is far from reality. In fact, if each building roof in a grid was painted with high-reflectance material, the reflected solar radiation could be absorbed by neighboring structures, also changing the energy balance of the urban area. In addition, the model used in this study treated the effects of the conversion of vegetation fraction on the $1 \times 1\,km^2$ areas, while the effects of detailed urban elements (*e.g.*, building aspect ratio, artificial heat flux, urban morphology, radiative effects on buildings, urban heterogeneity, and so on) were ignored, as we discussed in the previous section. Such effects could affect the ΔT_{smax} in each scenario. Although the meteorological model has limitations, knowledge about the regional variability of ΔT_{smax} is meaningful and finding that T_{smax} was decreased by the change of vegetation.

5. Conclusion

In this study, we investigated regional variability of impacts on future T_{smax} arising from land use change over the Kanto region, Japan. We introduced grid surface parameters (*i.e.*, albedo, heat capacity, and an evapotranspiration coefficient) in a meteorological model (JMANHM). The T_{smax} values calculated in the control simulation (*e.g.*, using current land use) agreed well with the observational AMeDAS data. Sensitivity experiments, in which land use was changed from urban to vegetated, validated the ability of the model to qualitatively reproduce the effects of land use change on surface air temperature. The experiments also indicated that while areas with the possibility of additional afforestation or GI are widely available in the western part of the Kanto region, such areas are less in the eastern part of the Kanto region.

Using different land use scenarios, we investigated the impacts of urban structure (*i.e.*, dispersed-city vs. compact-city) on T_{smax}. The results showed that a compact-city with active afforestation would be most effective in reducing high urban temperatures in the Kanto region, and that changing the albedo of urban infrastructure might also be a valid option for mitigating high urban temperatures in Tokyo.

In coastal areas (*e.g.*, Kanagawa), the impacts of land use change on T_{smax} were smaller than in inland areas. Sensitivity experiments showed that the impact of afforestation was mainly controlled

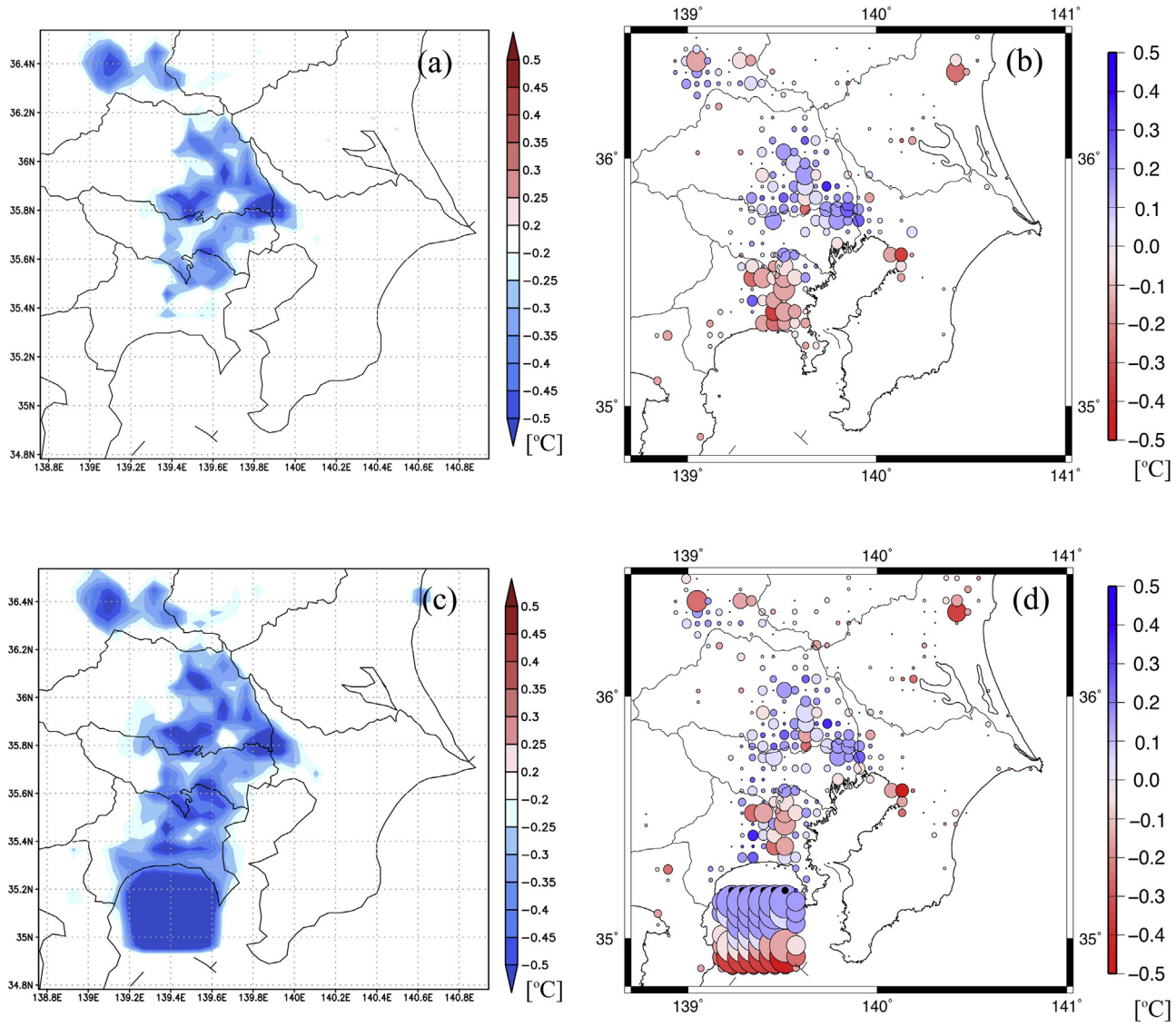

Fig. 11. Geographical distribution of the anomaly of mean daily maximum surface temperature (ΔT_{smax}) for each sensitivity experiment. Difference in daily maximum surface temperature in each sub domain ($5 \times 5\,km^2$ width) over the land between the (a) BAY-CTL scenario and the BAY-COMP30, and (c) BAY-CTL-SAGAMI and the BAY-COMP30 scenarios ($T_{smax,***} - T_{smax,BAY\text{-}CTL}$) averaged over the last 9 days of the simulation. Geographical distribution of afforestation (greening) ratio (G; shown by circle size) and the anomaly of ΔT_{smax} from the mean ΔT_{smax} between (b) the BAY-CTL and the BAY-COMP30, and (d) the BAY-CTL-SAGAMI and the BAY-COMP30 scenarios. To calculate G, the number of urban grids in BAY-CTL was used for U_p in Eq. (4). For scenario descriptions, see Table 3. (This figure is monochrome in printed version. For interpretation of the references to colour in this figure legend, the reader is referred to the web version of this article.)

by the total distance travelled by the prevailing air masses over afforested areas. This indicates that afforestation of coastal Kanagawa would contribute to the reduction of high urban temperatures in the inland areas of Saitama and Tokyo.

The results revealed that regional variability of afforestation with changing urban structure may be controlled by meteorological conditions. Information about such regional variability is crucial for effective afforestation and urban planning. The numerical simulations provided by meteorological modeling expressing land characteristics used in this study can supply helpful information toward sustainable design solutions.

Acknowledgement

This study was supported by projects from JAXA/EarthCARE, MEXT/VL for Climate System Diagnostics, the Global Environment Research Fund S-12 of the Ministry of the Environment (MOE) in Japan, NIES/GOSAT, NIES/CGER, MEXT/RECCA/SALSA. This work was carried out by the joint research program of CEReS, Chiba university (2015). This research was conducted using the HITACHI SR16000 System (yayoi) in the Information Technology Center, The University of Tokyo. The authors are thankful to Dr. S. A. Adachi of RIKEN, and Mr. M. Nagai of Chiba University for their useful comments and help with some of the analyses. Some of the figures were created by The Grid Analysis and Display System (GrADS), Gnuplot, and The Generic Mapping Tool (GMT). The first author is supported by RIKEN special postdoctoral research program.

Appendix A. Conversion from surface heat flux by vegetation flux

To unravel the physical mechanisms controlling T_{smax}, we considered the diurnal variations in surface temperatures, and latent and sensible heat flux for each land use type (Fig. A1). In terms of ΔT_{smax} magnitude, “cultivation” involved the largest variation, followed by “low tree and multi-year ground cover”, “low tree and

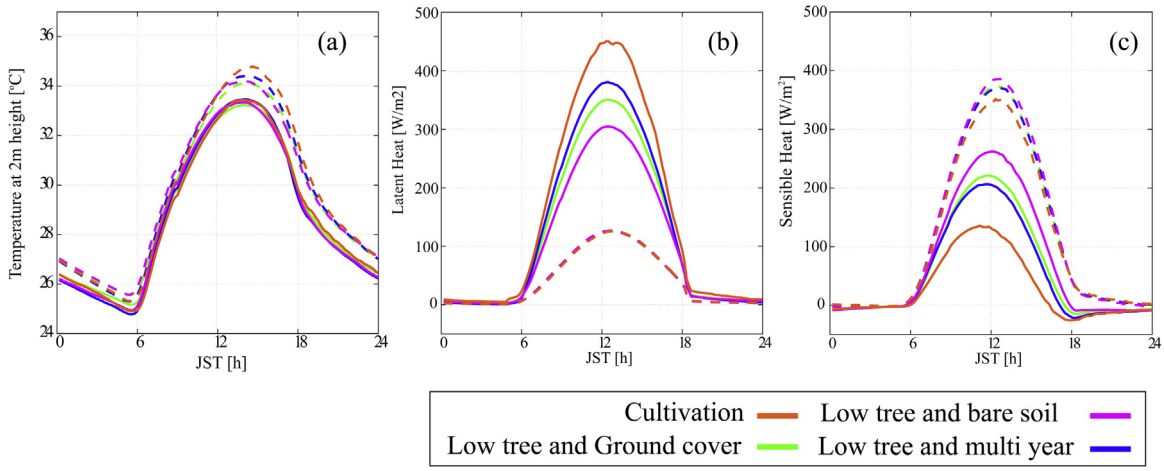

Fig. A1. Time series of T_{smax}, latent heat flux, and sensible heat flux. Temporal variations averaged over 9 days for (a) maximum temperature at 2 m height (T2m), (b) latent heat flux, and (c) sensible heat flux, averaged over all grids of each category whose land use was "urban" in CTL, in the (solid) VEG50 and (dashed) CTL scenarios. The results for the "forest" category were omitted owing to the extremely small number of grids. For scenario descriptions, see Table 3. (This figure is monochrome in printed version. For interpretation of the references to colour in this figure legend, the reader is referred to the web version of this article.)

Table A1
ΔT_{smax}, the difference of latent heat flux, and the difference of sensible heat flux between CTL and VEG50 (VEG50-CTL) at 14 JST for each category shown in Fig. A1, averaged over last 9 days of the simulation.

Category	ΔT_{smax} [°C]	Difference of latent heat flux [W m^{-2}]	Difference of sensible heat flux [W m^{-2}]
Low tree and bare soil	−0.847	165.05	−128.26
Low tree and ground cover	−0.872	208.13	−160.60
Low tree and multi-year ground cover	−0.938	232.02	−178.69
Cultivation	−1.26	306.17	−223.95

ground cover", and "low tree and bare soil" (*e.g.*, ΔT_{smax} at 14:00 Japan Standard Time (JST; 05:00 UTC), when T_{smax} usually occurred, are shown in Table A1). In the CTL urban land use, the daytime sensible heat flux in urban areas was larger than the latent heat flux. Contrarily, for VEG50 with vegetation land use, latent heat flux was larger than sensible heat flux. In terms of differences between CTL and VEG50, "cultivation" incurred the more pronounced heat flux, followed by "low tree and multi-year ground cover", "low tree and ground cover", and "low tree and bare soil"; this is the same order depicted by magnitudes of ΔT_{smax} (Table A1). This results from the difference in β between urban and vegetated land. Evapotranspiration was inactive in urban areas in CTL because of the small β (Table 2). In contrast, evapotranspiration was active in VEG50 with vegetated grids. The resulting variation in β provoked the conversion of sensible into latent heat flux, leading to the decrease in T_{smax} yielded by VEG50 simulation. This result is consistent with those of previous studies (*e.g.*, Kusaka et al., 2000).

As in the daytime case, nighttime temperatures were lower in the VEG50 simulation compared to CTL. This reflected the large heat capacity (C_h) of urban areas (Table 2) and was consistent with the results of Kondo (1994). Taken together, our findings showed that the model is able to reflect quantitatively the differences of T_{smax} between urban and vegetated areas.

References

Adachi, S.A., Kimura, F., Kusaka, H., Duda, M.G., Yamagata, Y., Seya, H., Nakamichi, K., Aoyagi, T., 2014. Moderation of summertime heat island phenomena via modification of the urban form in the Tokyo metropolitan area. J. Appl. Meteorol. Climatol. 53, 1886–1900, http://dx.doi.org/10.1175/JAMC-D-13-0194.1.

Adachi, S.A., Kimura, F., Kusaka, H., Inoue, T., Ueda, H., 2012. Comparison of the impact of global climate changes and urbanization on summertime future climate in the Tokyo metropolitan area. J. Appl. Meteorol. Climatol. 51, 1441–1454, http://dx.doi.org/10.1175/JAMC-D-11-0137.1.

Aoyagi, T., Seino, N., 2011. A square prism urban canopy scheme for the NHM and its evaluation on summer conditions in the Tokyo metropolitan area, Japan. J. Appl. Meteorol. Climatol. 50, 1476–1496, http://dx.doi.org/10.1175/2011JAMC2489.1.

Aoyagi, T., Kayaba, N., Seino, N., 2012. Numerical simulation of the surface air temperature change caused by increases of urban area anthropogenic heat, and building aspect ratio in the Kanto-Koshin area. J. Meteorol. Soc. Japn. 90B, 11–31, http://dx.doi.org/10.2151/jmsj.2012-B02.

Ariga, T., Matsuhashi, K., 2012. Development of formulation method for centralized and decentralized scenarios on regional population distribution—using mesh-based national population census – (in Japanese). J. City Plan. Inst. Japn. 47, 745–750.

Best, M.J., Grimmond, C.S.B., 2015. Key conclusions of the first international urban land surface model comparison project. Bull. Am. Meteorol. Soc. 96, 805–819, http://dx.doi.org/10.1175/BAMS-D-14-00122.1.

Brink, E., Aalders, T., Ádám, D., Feller, R., Henselek, Y., Hoffmann, A., Ibe, K., Matthey-Doret, A., Meyer, M., Negrut, N.L., Rau, A.L., Riewerts, B., von Schuckmann, L., Törnros, S., von Wehrden, H., Abson, D.J., Wamsler, C., 2016. Cascades of green: a review of ecosystem-based adaptation in urban areas. Glob. Environ. Chang. 36, 111–123, http://dx.doi.org/10.1016/j.gloenvcha.2015.11.003.

Conlon, K., Monaghan, A., Hayden, M., Wilhelmi, O., 2016. Potential impacts of future warming and land use changes on intra-urban heat exposure in Houston, Texas. PLoS One 11, e0148890, http://dx.doi.org/10.1371/journal.pone.0148890.

Emmanuel, R., Krüger, E., 2012. Urban heat island and its impact on climate change resilience in a shrinking city: the case of Glasgow, UK. Build. Environ. 53, 137–149, http://dx.doi.org/10.1016/j.buildenv.2012.01.020.

Gal-Chen, T., Somerville, R.C., 1975. On the use of a coordinate transformation for the solution of the Navier-Stokes equations. J. Comput. Phys. 17, 209–228, http://dx.doi.org/10.1016/0021-9991(75)90037-6.

U.S. Geological Survey, 1996. Global 30 Arc-Second Elevation (GTOPO30) [WWW Document]. URL https://lta.cr.usgs.gov/GTOPO30.

Haase, D., Haase, A., Rink, D., 2014. Conceptualizing the nexus between urban shrinkage and ecosystem services. Landsc. Urban Plan. 132, 159–169, http://dx.doi.org/10.1016/j.landurbplan.2014.09.003.

Japan Meteorological Agency, 2008. Climate change monitoring report 2007.

Kalnay, E., Kanamitsu, M., Kistler, R., Collins, W., Deaven, D., Gandin, L., Iredell, M., Saha, S., White, G., Woollen, J., Zhu, Y., Leetmaa, A., Reynolds, R., Chelliah, M., Ebisuzaki, W., Higgins, W., Janowiak, J., Mo, K.C., Ropelewski, C., Wang, J., Jenne, R., Joseph, D., 1996. The NCEP/NCAR 40-year reanalysis project. Bull. Am. Meteorol. Soc. 77, 437–471, http://dx.doi.org/10.1175/1520-0477(1996)077<0437:TNYRP>2.0.CO;2.

Kitagawa, Y., 2000. Radiation process (in Japanese). JMA nonhydrostatic model. Japn. Meteorol. Agency Annu. Rep. 46, 16–31.

Kondo, J., 1975. Air-sea bulk transfer coefficients in diabatic conditions. Boundary-Layer Meteorol. 9, 91–112, http://dx.doi.org/10.1007/BF00232256.

Kondo, J., 1994. Meteorology of Water Environment, 1st ed. Asakura Publishing Co., Ltd (In Japanese).
Krayenhoff, E.S., Voogt, J.A., 2010. Impacts of urban albedo increase on local air temperature at daily-annual time scales: model results and synthesis of previous work. J. Appl. Meteorol. Climatol. 49, 1634–1648, http://dx.doi.org/10.1175/2010JAMC2356.1.
Kusaka, H., Kimura, F., Hirakuchi, H., Mizutori, M., 2000. The effects of land-Use alteration on the sea breeze and daytime heat island in the tokyo metropolitan area. J. Meteorol. Soc. Japn. 78, 405–420, 0026-1165.
Kusaka, H., Hara, M., Takane, Y., 2012. Urban climate projection by the WRF model at 3-km horizontal grid increment: dynamical downscaling and predicting heat stress in the 2070's August for Tokyo, Osaka, and Nagoya metropolises. J. Meteorol. Soc. Japn. 90B, 47–63, http://dx.doi.org/10.2151/jmsj.2012-B04.
Kusaka, H., Suzuki-Parker, A., Aoyagi, T., Adachi, S.A., Yamagata, Y., 2016. Assessment of RCM and urban scenarios uncertainties in the climate projections for August in the 2050 in Tokyo. Clim. Change, http://dx.doi.org/10.1007/s10584-016-1693-2.
Louis, J.-F., 1979. A parametric model of vertical eddy fluxes in the atmosphere. Boundary-Layer Meteorol. 17, 187–202, http://dx.doi.org/10.1007/BF00117978.
Martilli, A., 2014. An idealized study of city structure, urban climate, energy consumption, and air quality. Urban Clim. 10, 430–446, http://dx.doi.org/10.1016/j.uclim.2014.03.003.
Monteith, J.L., 1965. Evaporation and environment. Symp. Soc. Exp. Biol. 19, 205–234.
Moriwaki, R., Kanda, M., Watanabe, T., Matsunaga, K., 2002. Estimation of land-surface parameters in urban boundary layer (In Japanese). Proc. Hydraul. Eng. 46, 91–96.
Nakanishi, M., Niino, H., 2006. An improved Mellor-Yamada level-3 model: its numerical stability and application to a regional prediction of advection fog. Boundary-Layer Meteorol. 119, 397–407, http://dx.doi.org/10.1007/s10546-005-9030-8.
National Land Information Division National Spatial Planning and Regional Policy Bureau MILT of Japan, 1997. National Land Numerical Information [WWW Document]. URL Downloaded from http://nlftp.mlit.go.jp/ksj-e/index.html.
Ng, C.F.S., Ueda, K., Ono, M., Nitta, H., Takami, A., 2014. Characterizing the effect of summer temperature on heatstroke-related emergency ambulance dispatches in the Kanto area of Japan. Int. J. Biometeorol. 58, 941–948, http://dx.doi.org/10.1007/s00484-013-0677-4.
Onishi, A., Cao, X., Ito, T., Shi, F., Imura, H., 2010. Evaluating the potential for urban heat-island mitigation by greening parking lots. Urban For. Urban Green. 9, 323–332, http://dx.doi.org/10.1016/j.ufug.2010.06.002.
Saito, K., Fujita, T., Yamada, Y., Ishida, J., Kumagai, Y., Aranami, K., Ohmori, S., Nagasawa, R., Kumagai, S., Muroi, C., Kato, T., Eito, H., Yamazaki, Y., 2006. The operational JMA nonhydrostatic mesoscale model. Mon. Weather Rev. 134, 1266–1298, http://dx.doi.org/10.1175/MWR3120.1.
Sakurai, M., Shinohara, Y., Mashimo, K., Sunaga, T., 2009. High temperature in 2007 when the daily maximum temperature was over 40 °C: part 1 analyses for 15 and 16 of August 2007 (in Japanese). TENKI 56, 248–253.
Skamarock, W. C., Coauthors, 2008: A description of the advanced research WRF version 3. NCAR Tech. Note NCAR/TN-4751STR, 113 pp. [WWW Document] URL Downloaded from http://www2.mmm.ucar.edu/wrf/users/docs/arw_v3.pdf.
Scherer, D., Fehrenbach, U., Beha, H., Parlow, E., 1999. Improved concepts and methods in analysis and evaluation of the urban climate for optimizing urban planning processes. Atmos. Environ. 33, 4185–4193, http://dx.doi.org/10.1016/S1352-2310(99)00161-2.
Seto, K.C., Fragkias, M., Güneralp, B., Reilly, M.K., 2011. A meta-analysis of global urban land expansion. PLoS One 6, e23777, http://dx.doi.org/10.1371/journal.pone.0023777.
Shrestha, Kundan, L., Kondo, A., Maeda, C., Kaga, A., Yoshio, I., 2008. Investigating the contribution of urban canopy model and anthropogenic heat emission to urban heat island effect using WRF model. Japn. Soc. Refrig. Air Cond. Eng 26, 45–55.
Song, J., Wang, Z.-H., 2015. Interfacing the urban land-atmosphere system through coupled urban canopy and atmospheric models. Boundary-Layer Meteorol. 154, 427–448, http://dx.doi.org/10.1007/s10546-014-9980-9.
Stocker, T.F., Qin, D., Plattner, G.-K., Tignor, M., Allen, S.K., Boschung, J., Nauels, A., Xia, Y., Bex, V., Midgley, P.M., 2013. IPCC, 2013: Climate Change 2013: The Physical Science Basis, IPCC. Cambridge University Press, Cambridge, United Kingdom and New York, NY, USA.
Suzuki-Parker, A., Kusaka, H., Yamagata, Y., 2015. Assessment of the impact of metropolitan-scale urban planning scenarios on the moist thermal environment under global warming: a study of the tokyo metropolitan area using regional climate modeling. Adv. Meteorol. 2015, 1–11.
Takebayashi, H., Moriyama, M., 2012. Study on surface heat budget of various pavements for urban heat island mitigation. Adv. Mater. Sci. Eng. 2012, 1–11, http://dx.doi.org/10.1155/2012/523051.
Theeuwes, N.E., Steeneveld, G.J., Ronda, R.J., Heusinkveld, B.G., van Hove, L.W.A., Holtslag, A.A.M., 2014. Seasonal dependence of the urban heat island on the street canyon aspect ratio. Q. J. R. Meteorol. Soc. 140, 2197–2210, http://dx.doi.org/10.1002/qj.2289.
Tran, H., Uchihama, D., Ochi, S., Yasuoka, Y., 2006. Assessment with satellite data of the urban heat island effects in Asian mega cities. Int. J. Appl. Earth Obs. Geoinf. 8, 34–48, http://dx.doi.org/10.1016/j.jag.2005.05.003.
United Nations, 2015. World Urbanization Prospects: The 2014 Revision (ST/ESA/SER.A/352).
Wang, Z.-H., Bou-Zeid, E., Smith, J.A., 2013. A coupled energy transport and hydrological model for urban canopies evaluated using a wireless sensor network. Q. J. R. Meteorol. Soc. 139, 1643–1657, http://dx.doi.org/10.1002/qj.2032.
Yamada, Y., 2003. Cloud microphysics (in Japanese). JMA nonhydrostatic model. Japn. Meteorol. Agency Annu. Rep. 49, 52–76.
Yamagata, Y., Seya, H., Nakamichi, K., 2011. Scenario analysis of the future urban land use in the Tokyo metropolitan area. Environ. Sci. 24, 169–179, http://dx.doi.org/10.11353/sesj.24.169.
Yang, J., Wang, Z.H., 2014. Physical parameterization and sensitivity of urban hydrological models: application to green roof systems. Build. Environ. 75, 250–263, http://dx.doi.org/10.1016/j.buildenv.2014.02.006.
Yang, J., Wang, Z.-H., Chen, F., Miao, S., Tewari, M., Voogt, J.A., Myint, S., 2015. Enhancing hydrologic modelling in the coupled weather research and forecasting-urban modelling system. Boundary-Layer Meteorol. 155, 87–109, http://dx.doi.org/10.1007/s10546-014-9991-6.
Yang, L., Niyogi, D., Tewari, M., Aliaga, D., Chen, F., Tian, F., Ni, G., 2016. Contrasting impacts of urban forms on the future thermal environment: example of Beijing metropolitan area. Environ. Res. Lett. 11, 034018, http://dx.doi.org/10.1088/1748-9326.